Volume Title
ASP Conference Series, Vol. **Volume Number**
Author

The X-ray View of OB Star Wind Structure and Dynamics

David H. Cohen,[1]

[1]*Department of Physics and Astronomy, Swarthmore College, 500 College Ave., Swarthmore PA 19081, USA*

Abstract. High-resolution X-ray grating spectroscopy enables us to measure the kinematics and spatial distribution of the shock-heated wind plasma in O and early B stars, testing the predictions of the embedded wind shock scenario of massive star X-ray production. By fitting models to the resolved, Doppler broadened X-ray emission line profiles measured by the *Chandra* X-ray Observatory's grating spectrometer, we find an onset radius of X-ray production of roughly $R_o = 1.5R_*$ for the O supergiants, ζ Pup and HD 93129A. From the profile fitting we also find that the terminal velocity of the X-ray emitting plasma is consistent with that of the bulk, UV absorbing wind. We also use the X-ray emission line profiles to measure the wind mass-loss rates and break the degeneracy between mass-loss rate and clumping factor that affects traditional H_α and radio free-free diagnostics. We find clumping factors of order $f_{cl} = 10$, which also agrees with the simulations of the wind instability. And we find that clumping begins very close to the photosphere, significantly lower in the wind than the onset of X-ray production. For lower density B star winds, the X-ray emission lines are much narrower than in the O supergiants, and are inconsistent with the hot plasma sharing the kinematics of the bulk wind.

1. Introduction

The focus of this paper will be normal, effectively single, non-magnetic OB stars. In the context of the meeting's topic, circumstellar dynamics at high resolution, we will focus on the highly supersonic and structured stellar winds of O and early B stars, rather than the disks and magnetospheres that surround Be and Bp stars, respectively. And in terms of the wind structure, clumping, and dynamics, we will have to rely on spectroscopy, as X-ray imaging and interferometry do not currently achieve the high resolution that would be needed to measure the expected small-scale structure in the near-star acceleration region of these winds.

Moderate-to-high resolution X-ray spectroscopy with the diffraction grating arrays on *Chandra* and *XMM-Newton* has been producing results on OB stars for the past decade. In this review, we will show how X-ray spectral diagnostics, in conjunction with modeling and numerical simulations can be used to address the following questions: (1) How is the hot ($T > 10^6$ K), X-ray emitting plasma produced in the wind? (2) What are its kinematics and spatial distribution? (3) What are the relationships among wind instabilities, X-ray production, and wind structure/clumping?

2. Data

The data we present here was taken with the High Energy Transmission Grating Spectrometer (HETGS) on the *Chandra X-ray Observatory* (Canizares et al. 2005). *Chandra*'s state-of-the-art X-ray optics produce a spatial resolution of $\sim 0.5''$, which is unprecedented (the ROSAT HRI had resolution of $5''$ (Truemper 1982)), and which will not be exceeded by any currently planned future mission. The sensitivity of the combined mirror assembly, HETGS, and ACIS CCD detector array is quite low, with an energy-dependent effective area of several tens of cm^2 from roughly 30 Å to 1.5 Å, although the sensitivity is quite poor at the short wavelength end and interstellar attenuation suppresses X-ray flux from distant O stars at the long wavelength end. The low sensitivity means that fewer than two-dozen O and early B stars have been observed with the *Chandra* gratings.

The HETGS consists of two grating arrays, with a factor of two difference in dispersion: the Medium Energy Grating (MEG) and the High Energy Grating (HEG). Their FWHM resolutions are 23 and 12 mÅ, respectively, corresponding to resolving powers of $\lambda/\Delta\lambda \approx 300$ to 1000 (1000 km s^{-1} to 300 km s^{-1}). Given wind velocities approaching and even exceeding 3000 km s^{-1} in early O stars, emission lines from hot plasma embedded in these stars' winds should be well resolved.

The *XMM* Reflection Grating Spectrometer has similar properties to the *Chandra* HETGS. The spatial resolution, internal noise, and calibration of *XMM* are not as good as *Chandra*'s, although the sensitivity is higher. Interesting results are being produced by the *XMM* RGS, but we will focus on the *Chandra* HETGS data here, primarily due to space limitations, although the constraints provided by *Chandra* data on OB star wind structure and dynamics are generally superior.

3. X-ray Emission From O Star Winds

The X-rays we see are from a low density ($n \sim 10^{10}$ cm^{-3}), collisional plasma, close to statistical equilibrium but far from LTE. In all of these senses, the hot, X-ray emitting plasma in OB star winds is similar to coronal plasma on solar-type stars. Indeed, the massive star community uses coronal spectral synthesis codes to model massive star X-ray spectra. The X-ray spectral emission properties of OB stars are described in the first subsection, below. The X-ray emitting plasma in nonmagnetic effectively single OB stars is assumed to be produced in embedded wind shocks (EWS) generated by the line-deshadowing instability (LDI), which we describe in the second subsection.

3.1. Thermal X-ray Emission

The low-density, quasi-steady-state nature of the X-ray emitting plasma means that nearly all of the ions have their bound electrons in the ground state configuration, and that collisional ionization is balanced by radiative and dielectronic recombination. Electrons, protons, and ions are assumed to be in thermal equilibrium, with each species having a Maxwellian velocity distribution. While these assumptions may be called into question under certain circumstances, there is no observational evidence for non-equilibrium effects in X-ray spectra (although photoionization out of metastable excited states can be important in helium-like species, and can, in fact, be used as a diagnostic of the location of the hot plasma with respect to the photosphere (Leutenegger et al. 2006)).

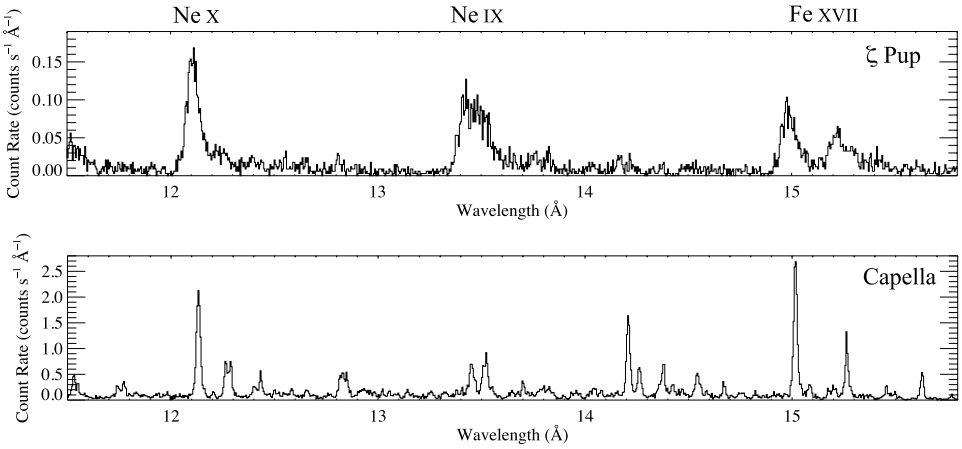

Figure 1. A portion of the *Chandra* MEG spectrum of the O supergiant ζ Pup is shown in the top panel, with the G star Capella in the bottom panel, for comparison. Capella's lines are unresolved, and so they indicate the instrumental resolution. Clearly, the emission lines in ζ Pup are significantly Doppler broadened. It can also be seen that the same lines are present in both star's spectra, and also that the higher ionization Ne x is weaker relative to Ne ix in ζ Pup than in Capella, indicating that the plasma temperature is lower for the O star.

The coronal approximation, steady-state spectral emission described above is computed for millions of transitions in, for example, the Astrophysical Plasma Emission Code (APEC) (Smith et al. 2001). This code, and others like it, assume that the plasma is optically thin, so that the emergent spectrum is proportional to the emissivity. For O stars, with the densest winds, line optical depth effects – resonance scattering – can be important in some lines of the most abundant elements (Leutenegger et al. 2007), but overall this is a second-order effect. However, the cold, unshocked portion of the wind can be optically thick (in the bound-free continuum) to the X-ray emission from EWSs (Leutenegger et al. 2010).

The spectra synthesized with the coronal codes match observed X-ray spectra quite well. They are dominated by a small number of emission lines from hydrogen-like and helium-like ionization stages of abundant elements such as N, O, Ne, Mg, Si, S and L-shell emission from Fe; primarily Fe xvii. Carbon's contributions are generally outside of the effective *Chandra* bandpass, while H and He are fully ionized and do not contribute to the X-ray line emission. The emission lines are superimposed on a weak continuum due to bremsstrahlung and, to a lesser extent, recombination radiation. At temperatures above 30 MK or so, most abundant elements are fully ionized and line emission weakens and bremsstrahlung becomes dominant. A portion of the *Chandra* MEG spectrum of ζ Pup (O4If) is shown in Fig. 1.

Fitting the observed *Chandra* grating spectra with APEC models yields plasma temperature distributions and, in principle, abundances; both, effectively, from fitting line strength ratios. While significant nitrogen enhancement and oxygen depletion can be seen in the X-ray spectra of some O stars, in general, detailed abundance determinations cannot be reliably made from the X-ray data.

3.2. Embedded Wind Shocks

For the effectively single O and early B stars that are the focus of this paper, the X-ray emitting plasma is thought to be formed in numerous shock structures distributed throughout the wind. The lack of observed X-ray time variability suggests that there are (at least) hundreds of sites of X-ray production in a given wind. We do note that in some close O+O and WR binaries, wind-wind interactions can lead to stronger and usually harder X-ray emission, often modulated on the orbital period, and for some magnetic O stars, wind channeling can also lead to stronger and harder X-ray emission. While quite interesting, discussion of these two alternate mechanisms is beyond the scope of this paper (see review by Güdel & Nazé (2009)). However, we will note that X-rays from the binary wind interaction region can be spatially resolved in Chandra X-ray images of at least one massive star, WR 147 (Zhekov & Park 2010).

The mechanism that produces the wind shocks in normal, effectively single O and early B stars is the line-deshadowing instability, in which the ions that mediate the momentum transfer from the photospheric radiation field to the wind via resonance line scattering move out of the Doppler shadow of the slower moving, less blue-shifted material below them and are thus exposed to more driving radiation. This increases their velocity, further deshadowing them. In this manner, fast-moving rarefied streams flow into slower-moving, denser downstream structures (Milne 1926; Lucy & White 1980; Owocki et al. 1988). The sound speed in O star winds, which have temperatures of order 10^4 K, is only 10 or 20 km s^{-1}, and so these interactions are likely to lead to shock heating. For a solar abundance perfect gas a shock jump velocity of about 300 km s^{-1} heats plasma to $T \approx 10^6$ K, and the temperature scales as the square of the shock jump velocity.

Numerical radiation-hydrodynamics simulations of O star winds that include full, non-local radiation transport (and thus "automatically" include the LDI) show relatively smooth wind flows for the first few tenths of a stellar radius (understood in terms of the line-drag effect due to the strong electron-scattered radiation field near the base of the wind). But at about $r = 1.5R_*$ shocks quickly develop and dense clumps are produced, with faster rarefied flows slamming into them, producing moderately strong reverse shocks, generally of 500 km s^{-1} or less (Runacres & Owocki 2002). This comports with the temperatures of a few million K inferred from APEC modeling of O star grating spectra (Wojdowski & Schulz 2005; Nazé et al. 2012). For the denser winds of O supergiants, the shock cooling lengths should be relatively short and the shocks should be radiative. For the low density winds of early B stars, the cooling lengths may exceed the local radius and thus we may expect wind shocks in these stars to be primarily adiabatic.

The LDI is quite robust, and produces wind structure even when the instability is not seeded. Presumably round-off error in the numerical hydro scheme effectively seeds the instability. However, such simulations generally do not produce enough X-rays. Feldmeier et al. (1997) therefore performed simulations with turbulence imposed at the lower wind boundary. They found increased X-ray production, mostly due to clump-clump collisions. All of the published simulations that include an energy equation in order to compute X-ray emission are one-dimensional. This severe limitation is necessitated by the expense of the radiation transport in the hydrodynamics code. The geometry dictates that clumps are in fact spherical shells. This significantly limits that shock dynamics, and probably artificially inflates the clump spacing and perhaps affects the strengths of the shocks and the total mass flux through shocks. Exploratory

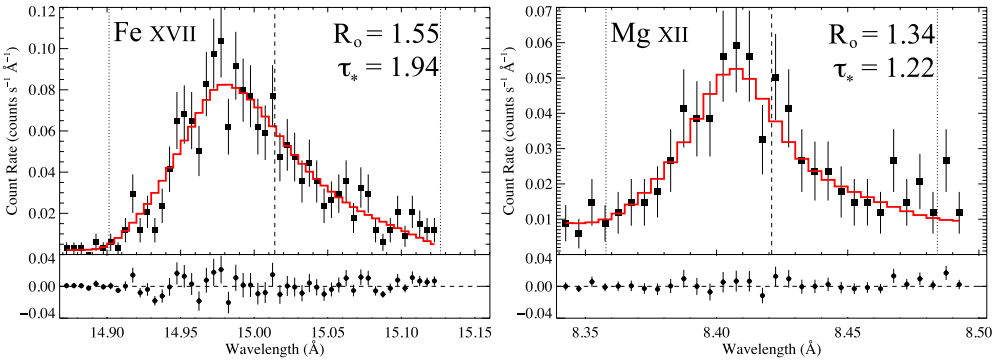

Figure 2. The Fe XVII line at 15.014 Å (left) and Mg XII Lyα line measured in ζ Pup with the *Chandra* MEG. in each panel the laboratory rest wavelength is indicated by the vertical dashed line, and the two dotted lines represent the Doppler shifts associated with $\pm v_\infty$. The best-fit model is indicated by the red histogram.

2-D simulations have been performed in the last decade, and these show Rayleigh-Taylor breakup of shells and the formation of very small clumps (Dessart & Owocki 2005). Thus far, these 2-D simulations have not included an energy equation and thus predictions of X-ray properties are lacking.

There is clearly much work to be done on the LDI and on the properties of O star wind shocks from the theoretical and numerical side. But the basic predictions of the EWS scenario and the LDI simulations can be tested with the *Chandra* and *XMM* grating spectra. These predictions include: shock heated plasma sharing the overall kinematics of the wind; an X-ray onset at several tenths of a stellar radius, thus implying that all X-ray emitting plasma will be traveling at an appreciable fraction of the wind terminal velocity; and the formation of clumps with an overdensity corresponding to $f_{\rm cl} \approx 10$, where the clumping factor, $f_{\rm cl} \equiv \langle\rho^2\rangle/\langle\rho\rangle^2$. Information about these kinematic and spatial properties can be determined from the observed X-ray line profiles. Furthermore, simulations predict that only a small fraction of the wind is shock heated, and so the colder bulk wind should absorb the shock-produced X-rays.

In the next section, we examine what we can learn from line profile modeling, in terms of wind shock kinematics, mass-loss rates, and clumping properties of the O supergiants, ζ Pup (O4 If) and HD 93129A (O2 If*).

4. X-ray Emission Line Profile Analysis

We use the Owocki & Cohen (2001) profile model, which assumes the same β velocity law for the bulk wind and the X-ray emitting plasma, and assumes a sudden X-ray onset at $r = R_{\rm o}$ with X-ray emission above that scaling with the square of the wind density. The larger the $R_{\rm o}$ parameter is, the broader the line, as more of the hot plasma is moving with velocities close to v_∞. For exceptionally high signal-to-noise lines, we can allow v_∞ to also be a free parameter, although it usually is fixed at the value observed in UV lines for the bulk wind. The effect of wind attenuation is to preferentially absorb photons from the red wing of the emission line, because those photons are produced in the receding back hemisphere of the wind. In the context of this spherically symmetric model, one parameter, $\tau_* \equiv \kappa \dot{M}/4\pi R_* v_\infty$, describes the degree of attenuation.

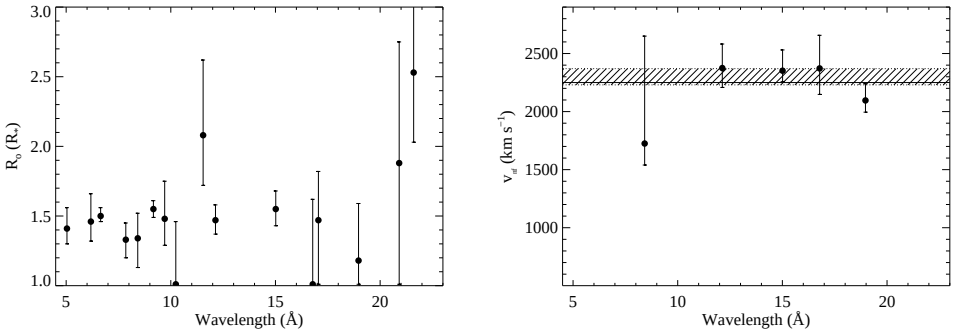

Figure 3. The fitted shock onset radii (left) and terminal velocities (right) for ζ Pup. The cross-hatched region on the terminal velocity plot represents the 68 percent confidence limits on the average terminal velocity derived from the five line fits, while the solid horizontal line represents the UV wind terminal velocity.

Profile models with R_o, τ_*, the line flux, and sometimes v_∞ as free parameters are fit to each line in the *Chandra* grating spectrum of a given star. Details of the procedure and a discussion of the sensitivity of the derived parameters to various modeling assumptions and uncertainties are discussed in Cohen et al. (2010). Two representative fits – to the Fe XVII line at 15.014 Å and to the Mg XII Lyα line in the *Chandra* MEG spectrum of ζ Pup – are shown in Fig. 2. Both lines are significantly Doppler broadened, consistent with X-ray onset radii, R_o, several tenths of a stellar radius above the photosphere.

We obtain similar results for the other fourteen lines in the *Chandra* HETGS spectrum of ζ Pup. The results are summarized in Fig. 3, where it can be seen that the line widths are consistent with a single value of $R_o \approx 1.5R_*$. For five of the higher signal-to-noise lines, the terminal velocity was allowed to be a free parameter of the fit, and those results are also summarized in that same figure. They are consistent with the UV wind terminal velocity of $v_\infty = 2250$ km s^{-1}.

The two lines shown in Fig. 2 both have wind absorption signatures, with a deficit of red-shifted counts leading to a net blue-shift and skewness. The degree of wind attenuation is greater in the longer wavelength Fe XVII line, as is expected from the trend in the wavelength-dependent opacity. Indeed, this enables us to fit a group of τ_* values derived for a given star with a single mass-loss rate, $\dot{M}$. Such an X-ray-based mass-loss rate determination is not susceptible to uncertainties due to density-squared clumping effects. In fact, by combining this (column) density sensitive X-ray mass-loss rate with the density-squared mass-loss diagnostics such as Hα or radio free-free (which provide the quantity $\dot{M} f_{\rm cl}^{0.5}$), the clumping factor can effectively be measured.

In Fig. 4 we show the distribution of τ_* values for the sixteen lines we fit in the *Chandra* HETGS spectrum of ζ Pup. The run of τ_* vs. wavelength, corresponding to the best-fit mass-loss rate, is also shown. That value – 3.5×10^{-6} M$_\odot$ yr^{-1} – is about a factor of 2.5 below the unclumped Hα value, implying a clumping factor in the Hα formation region of $f_{\rm cl} \approx 6$ (but smaller clumping factors farther out in the wind (Puls et al. 2006)). Interestingly, in order to fit the observed Hα profile, the clumping must start at 1.1 R_*, while the X-ray plasma exists only above 1.5 R_*.

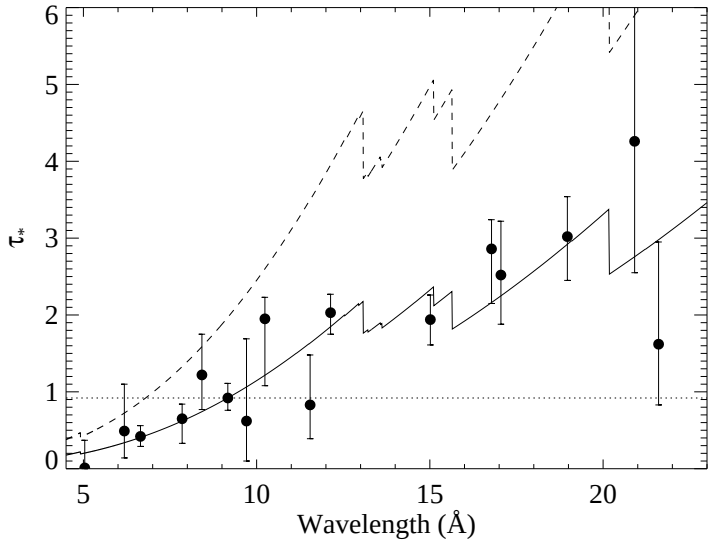

Figure 4. The fitted τ_* values for ζ Pup (left), along with the mass-loss rate fit (solid line) and the run of $\tau_*(\lambda)$ expected for the higher mass-loss rate that does not account for clumping (dashed line). The best constant τ_* is also shown (dotted line). Neither of these latter two models provides a good fit to the values derived from the data.

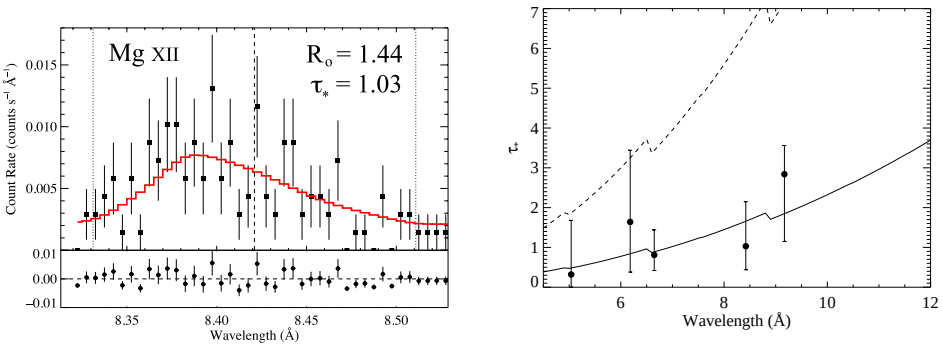

Figure 5. The Lyman-α line of Mg XII in HD 93129A (left) shows a similar blue-shift and skewness as that seen in the same line in the ζ Pup spectrum (Fig. 2). The derived mass-loss rate for this star is about 7×10^{-6} $M_\odot$ yr^{-1} (solid line, right panel), two times larger than the value we determine for ζ Pup, but almost four times lower than the unclumped Hα mass-loss rate (dashed line).

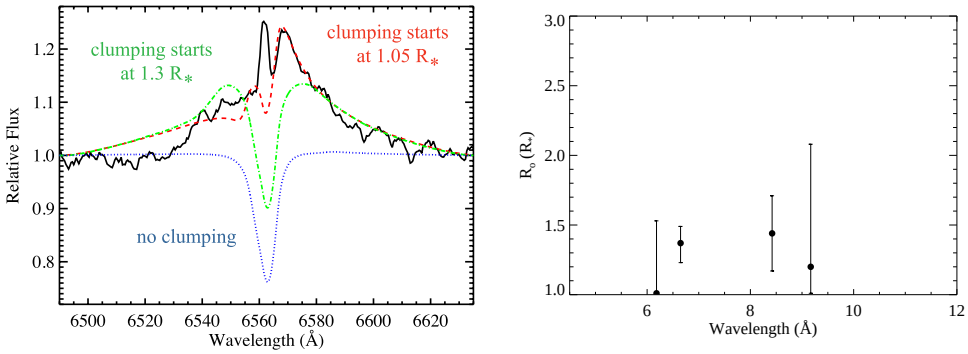

Figure 6. The Hα line in HD 93129A (black, solid; left panel) overplotted with several models. Note that the wind clumping must start very close to the photosphere in order to fit this line. The values of R_0 derived from fitting the lines in the *Chandra* spectrum are also shown (right panel); they are consistent with a value of $R_0 = 1.4R_*$ and inconsistent with the value of $r = 1.05R_*$ inferred for the clumping onset radius.

We obtain similar results, albeit with fewer lines, for the more distant O supergiant, HD 93129A (O2 If*), which also shows broadened, asymmetric emission lines in its *Chandra* HETGS spectrum (Cohen et al. 2011). The Mg XII Lyman-α line is shown in Fig. 5, where we also show the mass-loss rate fit to the ensemble of τ_* values. We can simultaneously fit the Hα line in this star if we assume a clumping factor of $f_{\rm cl} = 12$, but the fit requires that clumping starts already at $R_{\rm cl} = 1.05R_*$, while the X-ray onset radius has a mean value of $R_0 = 1.4R_*$. These results are shown in Fig. 6.

In summary, the dense winds of the O supergiants ζ Pup and HD 93129A behave in accordance with the LDI-induced embedded wind shock scenario. These winds are moderately clumpy, with multi-million K shock-heated plasma distributed throughout the wind above about 1.5 R_* and with the same kinematics as the bulk wind.

However, when we look at a massive star with a much weaker wind, we see qualitatively different behavior. In contrast with the O supergiants, the early B star, β Cru (B0.5 III) has X-ray emission lines that are quite narrow (Cohen et al. 2008). In Fig. 7 we show the same Fe XVII line shown in Fig. 2 for ζ Pup. The line, while resolved in β Cru, is much narrower than is expected in the standard EWS scenario.

While the lines in the *Chandra* grating spectrum of β Cru are relatively narrow, we know from the He-like forbidden-to-intercombination line ratios that the hot plasma is well out in the wind flow (Cohen et al. 2008). Furthermore, we also know from the relatively high X-ray flux from β Cru that a large fraction of the wind mass is heated to X-ray emitting temperatures. All of these properties can be understood in the context of the large post-shock cooling lengths expected in low-density winds like that seen in β Cru. The large post-shock regions are highly ionized and therefore ill suited to being driven by the photospheric UV radiation field; hence the low post-shock velocities. In contrast, the post-shock plasma in radiative shocks, as in the wind of ζ Pup, quickly cools and recombines and thus can be effectively driven before decelerating appreciably. Furthermore, the large volume filling factor of hot, post-shock plasma in the wind of β Cru also explains the relatively high X-ray flux observed in that star.

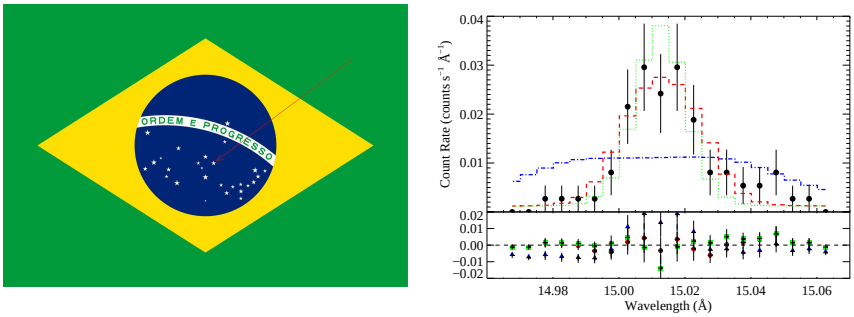

Figure 7. The early B star β Cru appears on the flag of the meeting's host nation, Brazil (left; red arrow). The Fe XVII line in β Cru, as seen in the *Chandra* MEG (right). The best-fit Gaussian line profile model is shown in red, and has a HWHM of 200 km s^{-1}. The green model is a delta function (convolved, like the other models, with the instrumental profile), while the blue model is what would be expected if the X-ray plasma has the same kinematics as the bulk wind. Clearly, this latter scenario, which holds for the O supergiants, can be ruled out for this star.

5. Conclusions

The X-ray emission observed from O stars with strong winds, and especially the high-resolution X-ray spectra, provide important confirmation of the general embedded wind shock scenario. The circumstellar dynamics determined from observations are consistent with the expectations of this scenario and, more specifically, the onset radii of X-ray emission derived from the *Chandra* line widths are consistent with simulations of embedded wind shocks due to the line-deshadowing instability. By combining X-ray absorption signatures in the emission line profiles with density-squared diagnostics at longer wavelengths, we are also able to measure the mass-loss rates and wind clumping factors in several O stars. The mass-loss rates agree with recent, lower determinations and the clumping factors, of order $f_{\rm cl} = 10$ agree with the predictions from numerical simulations of the LDI. However, we find that clumping starts very deep in the wind, closer to the photosphere than does the X-ray emission. It may be that the LDI produces the clumps deep in the wind, but that the associated wind flow speeds and shock jump velocities are not large enough to produce hot, X-ray emitting plasma. Or it may be that the clumps deep in the wind are produced by some mechanism other than the LDI.

For the winds of early B stars, with have densities roughly three orders of magnitude smaller than O supergiants, the X-ray lines observed with *Chandra* are quite narrow. Additionally, the X-ray fluxes are relatively high, given the low mass-loss rates. One scenario that could explain these properties is motivated by the large radiative cooling lengths associated with low-density wind shocks. Shocks in the winds of early B stars such as β Cru may be adiabatic, and once a parcel of wind material is shock heated (perhaps by the LDI), it remains hot and ionized as it traverses the large post-shock cooling region, failing to be further accelerated and leading to the rather modest Doppler broadening seen in the X-ray lines of B stars, and also leading to the large observed X-ray filling factors.

Acknowledgments. We acknowledge support from NASA grant NNX11AD26G to Swarthmore College.

References

Canizares, C. R., Davis, J. E., Dewey, D., Flanagan, K. A., Galton, E. B., Huenemoerder, D. P., Ishibashi, K., Markert, T. H., Marshall, H. L., McGuirk, M., Schattenburg, M. L., Schulz, N. S., Smith, H. I., & Wise, M. 2005, PASP, 117, 1144. arXiv:astro-ph/0507035

Cohen, D. H., Gagné, M., Leutenegger, M. A., MacArthur, J. P., Wollman, E. E., Sundqvist, J. O., Fullerton, A. W., & Owocki, S. P. 2011, MNRAS, 415, 3354. 1104.4786

Cohen, D. H., Kuhn, M. A., Gagné, M., Jensen, E. L. N., & Miller, N. A. 2008, MNRAS, 386, 1855. 0802.4084

Cohen, D. H., Leutenegger, M. A., Wollman, E. E., Zsargó, J., Hillier, D. J., Townsend, R. H. D., & Owocki, S. P. 2010, MNRAS, 405, 2391. 1003.0892

Dessart, L., & Owocki, S. P. 2005, A&A, 437, 657. arXiv:astro-ph/0503514

Feldmeier, A., Puls, J., & Pauldrach, A. W. A. 1997, A&A, 322, 878

Güdel, M., & Nazé, Y. 2009, A&A Rev., 17, 309. 0904.3078

Leutenegger, M. A., Cohen, D. H., Zsargó, J., Martell, E. M., MacArthur, J. P., Owocki, S. P., Gagné, M., & Hillier, D. J. 2010, ApJ, 719, 1767. 1007.0783

Leutenegger, M. A., Owocki, S. P., Kahn, S. M., & Paerels, F. B. S. 2007, ApJ, 659, 642. arXiv:astro-ph/0610181

Leutenegger, M. A., Paerels, F. B. S., Kahn, S. M., & Cohen, D. H. 2006, ApJ, 650, 1096. arXiv:astro-ph/0606370

Lucy, L. B., & White, R. L. 1980, ApJ, 241, 300

Milne, E. A. 1926, MNRAS, 86, 459

Nazé, Y., Flores, C. A., & Rauw, G. 2012, A&A, 538, A22. 1112.0862

Owocki, S. P., Castor, J. I., & Rybicki, G. B. 1988, ApJ, 335, 914

Owocki, S. P., & Cohen, D. H. 2001, ApJ, 559, 1108. arXiv:astro-ph/0101294

Puls, J., Markova, N., Scuderi, S., Stanghellini, C., Taranova, O. G., Burnley, A. W., & Howarth, I. D. 2006, A&A, 454, 625. arXiv:astro-ph/0604372

Runacres, M. C., & Owocki, S. P. 2002, A&A, 381, 1015

Smith, R. K., Brickhouse, N. S., Liedahl, D. A., & Raymond, J. C. 2001, ApJ, 556, L91. arXiv:astro-ph/0106478

Truemper, J. 1982, Advances in Space Research, 2, 241

Wojdowski, P. S., & Schulz, N. S. 2005, ApJ, 627, 953. arXiv:astro-ph/0503430

Zhekov, S. A., & Park, S. 2010, ApJ, 721, 518. 1007.4352

Questions

Ramiro de la Reza You mentioned that in the case of wind collisions in binaries the X-ray radiation can increase. Do you mean that new emission lines appear? That there is emission of hard X-rays?

David Cohen Yes, as the stars approach periastron, the X-ray flux generally increases and often, but not always, hardens, too.

Jose Groh Do you have long-term monitoring of the X-ray lines of ζ Pup? Would you expect variability based on the hydro simulations?

David Cohen The *Chandra* data covers less than a day, while there is almost a million seconds of *XMM* data. The *XMM* data shows no variability at the few percent level, implying under the most generic assumptions and using Poisson statistics, that there are several hundred sites of X-ray production in the wind. They must have relatively small lateral scale. In the 1-D simulations only a few locations at any given time are shock-heated because there's only so much variation that can be packed into the radial direction over the 10 to 100 R_* computational domain that is typically used. And those 1-D simulations do show a lot of variability; hence the inference about the small lateral scale.

Jon Bjorkman A number of years ago I worked on a crazy paper where we suggested that the red shifted absorption in the O VI lines of τ Sco was produced by infalling blobs. In your talk you suggested that the shocks in B star winds are adiabatic and that the collisional ionization will shut off the CAK line driving. What is the wind speed when this occurs? If this is less than the local escape speed, then this material would fall back onto the star. So this could be a possible mechanism for creating such infalling blobs in τ Sco.

David Cohen This is certainly an interesting idea, and τ Sco has a complex magnetic field and harder and stronger X-ray emission than typical early B stars (and narrow emission lines, too). τ Sco is also unusual, if not unique, in showing red shifted UV absorption. More generally, I think there would be ram pressure from the upstream wind flow pushing on "stalled" shocked gas. To answer your question directly, the wind flow speeds where the X-rays turn on are of order the local escape speed, so it is definitely something to consider.